

## Neutron irradiation and polarization effect of 4H–SiC Schottky detector

Ze Long<sup>a,b</sup>, Xiaochuan Xia<sup>a</sup>, Wei Jiang<sup>b,c</sup>, Hantao Jing<sup>b,c</sup>, Xinbo Zou<sup>d</sup>, Xin Shi<sup>c</sup>, Mengchen Niu<sup>a,b</sup>, Hongwei Liang<sup>a</sup>, Ruirui Fan<sup>b,c,e,\*</sup>

<sup>a</sup> School of Integrated Circuits, Dalian University of Technology, Dalian, 116620, PR China

<sup>b</sup> Spallation Neutron Source Science Center, Dongguan, 523803, PR China

<sup>c</sup> Institute of High Energy Physics, Chinese Academy of Sciences, Beijing, 100049, PR China

<sup>d</sup> School of Information Science and Technology, ShanghaiTech University, Shanghai, 201210, PR China

<sup>e</sup> State Key Laboratory of Particle Detection and Electronics, Institute of High Energy Physics, Chinese Academy of Sciences, Beijing, 100049, PR China



### ARTICLE INFO

#### Index Terms:

4H-SiC  
Detector  
Polarization effect  
Neutron irradiation

### ABSTRACT

Neutron irradiation experiments were carried out on a 4H–SiC Schottky detector. The effects of neutron and accompanying  $\gamma$ -rays irradiation on the electrical properties, charge collection efficiency (CCE), energy resolution and crystal defects of 4H–SiC detectors were investigated. The total irradiation fluence was  $1.24 \times 10^{14} \text{ n}/\text{cm}^2$ , with an equivalent 1 MeV neutron fluence of  $1.33 \times 10^{15} \text{ n}/\text{cm}^2$ . Following neutron irradiation, the turn-on voltage increased significantly, and the capacitance of the Schottky junction no longer varied with the reverse bias voltage. The CCE of the detector decreased from 100% to 90.8%, while the energy resolution increased from 0.79% to 1.49%. The irradiated detector required a higher bias voltage for optimal performance. Additionally, we observed two defect levels,  $E_c$ -0.5 eV and  $E_c$ -0.35 eV, in the 4H–SiC crystals after irradiation. Their generation is also related to gamma ray irradiation. The detector exhibited a polarization effect, where the energy spectrum split into two distinct components during prolonged measurement of monoenergetic  $\alpha$  particles. The peak position gradually shifted towards the lower energy side with increasing testing time. These effects can be mitigated by increasing the bias voltage to enhance the electric field strength in the drift region.

### 1. Introduction

In recent years, there has been considerable interest in 4H–SiC, a wide bandgap semiconductor material. The Schottky detectors made from 4H–SiC demonstrate excellent energy resolution, comparable to widely used Si detectors. One of the key advantages of the 4H–SiC detector is its high radiation tolerance and thermal stability [1–5]. These properties make it well-suited for various applications, including accelerator beam monitoring, nuclear physics data measurement, and nuclear reactor power monitoring [5–9]. 4H–SiC detectors have strong radiation resistance, and can maintain a stable operational state even under high doses of neutron, proton, and gamma radiation [10]. Ruddy and Seidel [11,12] irradiated 4H–SiC Schottky diodes to a cumulative  $^{137}\text{Cs}$  gamma-ray dose of 22.7 MGy. The irradiated detector was found to perform well as a detector for fast  $^{252}\text{Cf}$  fission neutrons and 14-MeV D-T neutrons [12]. Dulloo et al. [13] showed that the thermal-neutron response of a 4H–SiC Schottky diode with a  $^{6}\text{LiF}$  converter foil was indistinguishable from that of an unirradiated detector after a

fast-neutron ( $E > 1$  MeV) fluence of  $1.3 \times 10^{16} \text{ cm}^{-2}$ . These studies demonstrate the potential of 4H–SiC in the field of radiation-resistant detectors.

The 4H–SiC detectors developed by our research team have been effectively employed in the Back-n beamline of the China Spallation Neutron Source (CSNS). These detectors were utilized for measuring the differential cross-sections of different (n, lcp) nuclear reactions [14]. Remarkably, the detectors showed no degradation in performance even under neutron irradiation of  $1.05 \times 10^{13} \text{ n}/\text{cm}^2$  (1 MeV neutron). In order to further explore the degradation characteristics of the 4H–SiC detector at higher radiation doses, the neutron irradiation fluence was increased to  $1.24 \times 10^{14} \text{ n}/\text{cm}^2$ .

Previous studies have mainly focused on the degradation of electrical characteristics, CCE, energy resolution, and crystal defects as a result of radiation damage in 4H–SiC detectors [3,5,6,8]. This includes various particle radiation damage effects such as gamma rays [11,12], electrons, neutrons, protons [15], and heavy ions [16,17].

A typical work is the neutron irradiation experiment on 4H–SiC

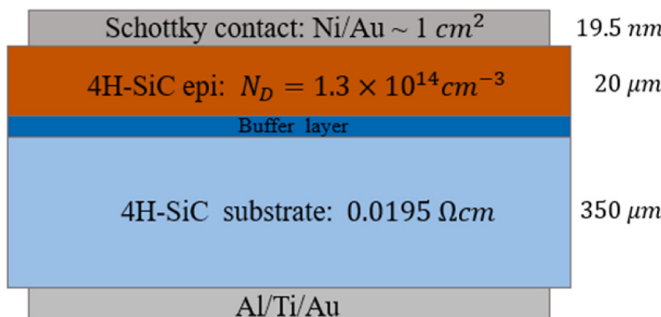
\* Corresponding author.

E-mail addresses: [hqliang@dlut.edu.cn](mailto:hqliang@dlut.edu.cn) (H. Liang), [fanrr@ihep.ac.cn](mailto:fanrr@ihep.ac.cn) (R. Fan).

**Table 1**

Other deep levels detected in 4H-SiC material.

Level	$E_C-E_T$ (eV)	$\sigma_n$ ( $\text{cm}^2$ )
S2	0.75	$1 \times 10^{-14}$
RD <sub>1/2</sub>	0.88	$3 \times 10^{-14}$
EH4	1.03	$2 \times 10^{-13}$
EH5	1.08	$2 \times 10^{-15}$
EH6/EH7	1.58	$6 \times 10^{-13}$

**Fig. 1.** Schematic diagram of the 4H-SiC Schottky detector.

detectors using the K600 Neutron Generator at the China Institute of Atomic Energy (CIAE) in Beijing, China [18]. The irradiation fluence is in the range of  $1.7 \times 10^{14} \text{ n/cm}^2$ . The energy resolution of the detector is about 2.4% before irradiation, with a saturated CCE of 100%. After neutron irradiation with  $1 \times 10^{14} \text{ n/cm}^2$  and  $7 \times 10^{14} \text{ n/cm}^2$ , the energy resolution of the detector decreased to 2.8% and 3.2%, and the CCE decreased to 95% and 90%. They also conducted higher fluence neutron irradiation experiments on 4H-SiC detectors using the Xi'an pulsed reactor at the Northwest Institute of Nuclear Technology (NINT) in Xi'an, China [19]. The total neutron irradiation fluence reached the level of  $1 \times 10^{16} \text{ n/cm}^2$ . This study demonstrates that 4H-SiC detectors can maintain their detection capability under  $1 \times 10^{16} \text{ n/cm}^2$  neutron irradiation. In addition, other studies have been conducted under neutron irradiation conditions in the range of  $1 \times 10^{13}$  to  $1 \times 10^{16} \text{ n/cm}^2$  and the results all indicate that 4H-SiC detectors have strong radiation resistance [20–25].

Research on defects in 4H-SiC crystal mainly focuses on the native defect Z<sub>1/2</sub> and its related derived defects in 4H-SiC epitaxial materials. Its energy level is E<sub>C</sub>-0.67 eV, and the most likely defect structure is the carbon vacancy (V<sub>C</sub>) defect. Some literature has studied the charge states of this defect structure and found that the energy levels corresponding to Z<sub>1</sub><sup>0/+</sup> and Z<sub>2</sub><sup>0/+</sup> are E<sub>C</sub> -0.52 eV and E<sub>C</sub> -0.42 eV, respectively, which can be generated by irradiation with 470 nm light [26–29]. In addition, defects at 0.25 eV, 0.38 eV, and 0.60 eV below the conduction band have been reported [30,31]. These defects can be generated by irradiation with various particles such as electrons, protons, neutrons, and alpha particles and are usually present simultaneously. The report

speculates that the possible sources of these defects are complex defects of impurity-vacancy atoms or vacancies in the material. Additionally, some deeper levels have also been detected, and the summarized results are shown in Table 1 [30].

Research on the polarization effect of 4H-SiC detectors is still relatively scarce, with only a few studies reporting the existence of polarization effects in current-type 4H-SiC detectors. More reports have focused on the diamond detectors in radiation measurements. The main experimental phenomenon is that during long-term measurements, the amplitude of the detector's output signal decreases with time, leading to a decrease in the count rate [32–35]. Therefore, in this study, we conducted comprehensive evaluations of these influencing factors. Additionally, we observed the occurrence of polarization effects. This study presents the first report on the polarization effects observed in neutron irradiated 4H-SiC Schottky detectors.

## 2. Fabrication of 4H-SiC detector and experimental setup

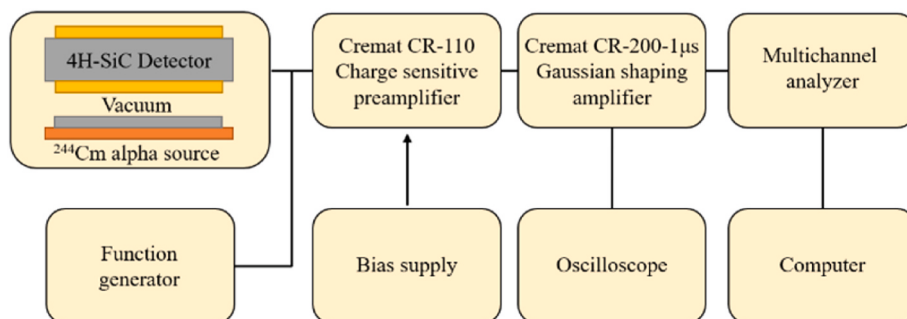
### 2.1. The structure of the 4H-SiC Schottky detector

We fabricated a 4H-SiC Schottky detector, and Fig. 1 shows the structure of the device. A 0.5 μm n<sup>+</sup> buffer layer was epitaxially grown onto a 350 μm n-type 4H-SiC substrate wafer. On the buffer layer, a 20 μm lightly doped epilayer was deposited with nitrogen doping concentration of  $1.3 \times 10^{14} \text{ cm}^{-3}$ . The ohmic contact was realized by the deposition of an Al/Ti/Au multilayer followed by annealing at 880 °C for 5 min in N<sub>2</sub>. The Schottky contact was formed on the surface of the epitaxial layer by the deposition of a 9.5 nm Ni film and a 10 nm Au film followed by annealing at 400 °C for 5 min in N<sub>2</sub>. The effective detection area of the detector is 1 cm<sup>2</sup>.

The detector can function under both unbiased and negatively biased voltage conditions. It has a saturation bias voltage of -60 V, resulting in a depletion region width of 20 μm. Alpha particles with energies of 6 MeV and lower can deposit their entire energy within this depletion region. The sensitive area of the detector is 1 cm<sup>2</sup>, and it possesses a thin dead layer with a thickness of only 19.5 nm. This thin dead layer significantly reduces the energy spread of incident particles and enhances the energy resolution of the detector.

### 2.2. Electrical and energy spectrum measurement system

The schematic of the α particles pulse-height spectrum measurement system is shown in Fig. 2. The system consists of a CREMAT CR110 Charge Sensitive Preamplifier (CSA), a CREMAT CR200-1μs Gaussian Shaping Amplifier, a multichannel analyzer (MCA), and power supply devices. To ensure proper functioning, the CSA and shaping amplifier are enclosed within a shielding box made of metal. For preamplifier testing and calibration, a Tektronix AFG31000 series function generator was employed. During spectroscopy measurements, the signals from the shaping amplifier are captured by the MCA, and subsequently, the data is analyzed using a computer.

**Fig. 2.** Schematic diagram of the α-particle energy spectrum measurement setup.

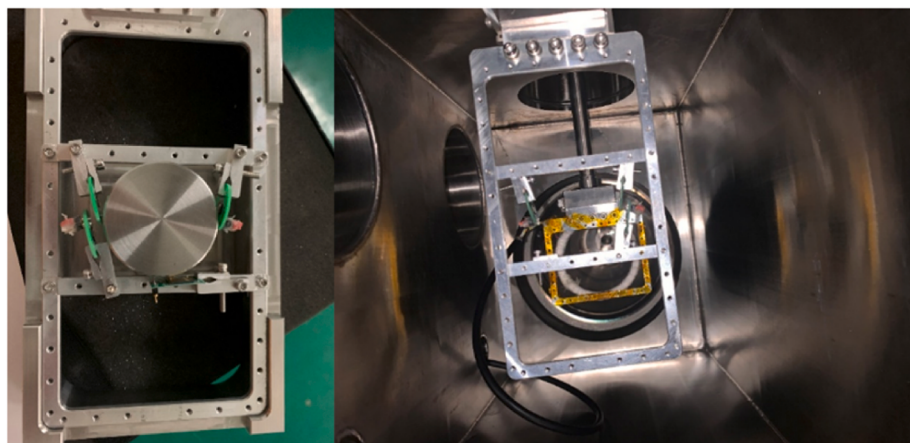


**Fig. 3.** Photographs of the CSNS Back-n neutron irradiation platform environment. The detector is fixed on the irradiation sample rack by a fixture, and it is suspended in the beam cavity. The picture on the right shows the interior of the irradiation cavity.

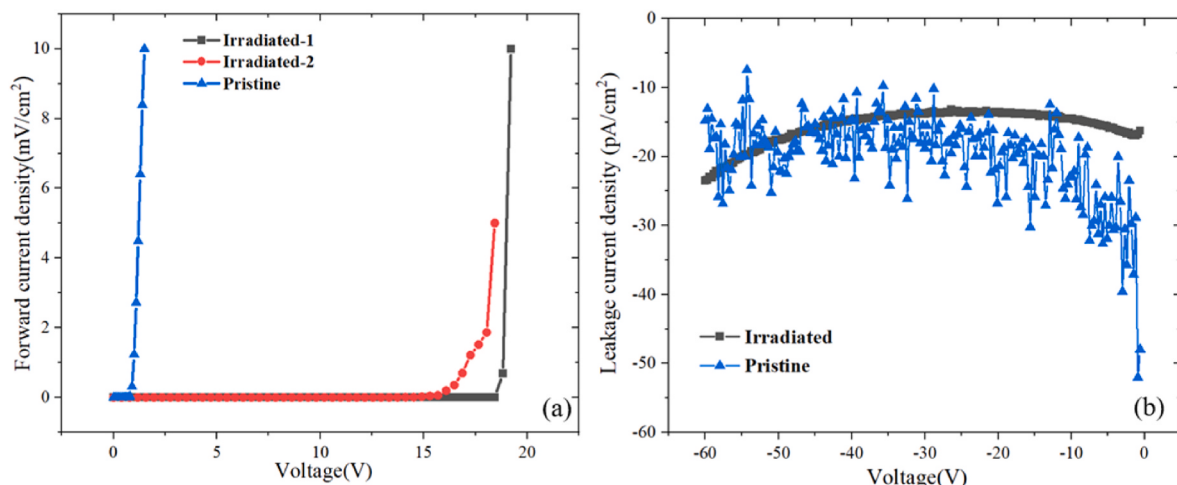


**Fig. 4.** J-V characteristics of the 4H-SiC detector before and after irradiation. (a) Forward J-V curves. (b) Reverse J-V curves.

The Current-Voltage (*J*-*V*) and Capacitance-Voltage (*C*-*V*) characteristics of the detector were acquired utilizing a Keysight B1505A Semiconductor Parameter Analyzer. All electrical measurements were

conducted at room temperature within a metal shielding box.

### 2.3. Neutron irradiation facility

The 4H-SiC detector was exposed to neutron irradiation at the back-n neutron irradiation platform of CSNS, as shown in Fig. 3. The energy spectrum of white neutrons at the CSNS back-n facility is in the range of 0.5 eV–200 MeV, with the neutrons penetrating through the entire detector [36]. After the detector underwent electrical measurements, spectral measurements, and defect-related measurements, it underwent neutron irradiation experiments. The irradiation process lasted for 313 h, with a fluence rate of  $1.1 \times 10^8$  n/cm<sup>2</sup>/s. The total fluence reached  $1.24 \times 10^{14}$  n/cm<sup>2</sup>, resulting in a total dose of 1740.8 Gy. The equivalent fluence for 1 MeV neutrons was  $1.33 \times 10^{15}$  n/cm<sup>2</sup>. Following the irradiation, the detector was placed in a lead shielding for 15 days and subsequently retrieved for testing. During this period, the storage environment temperature of the detector was approximately 300 K, and the detector may have been affected by the room temperature annealing effect.

## 3. Results and discussion

### 3.1. *J*-*V* and *C*-*V* measurement

The electrical characteristics of the detector were evaluated both

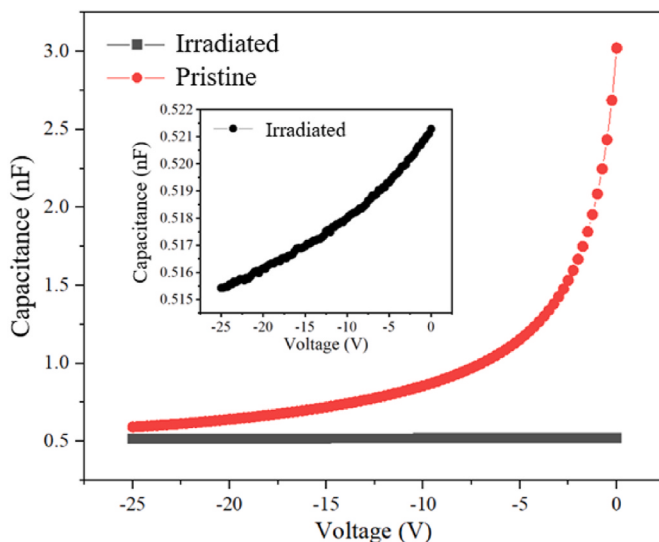


**Fig. 5.** C-V characteristics of the detector before and after irradiation.

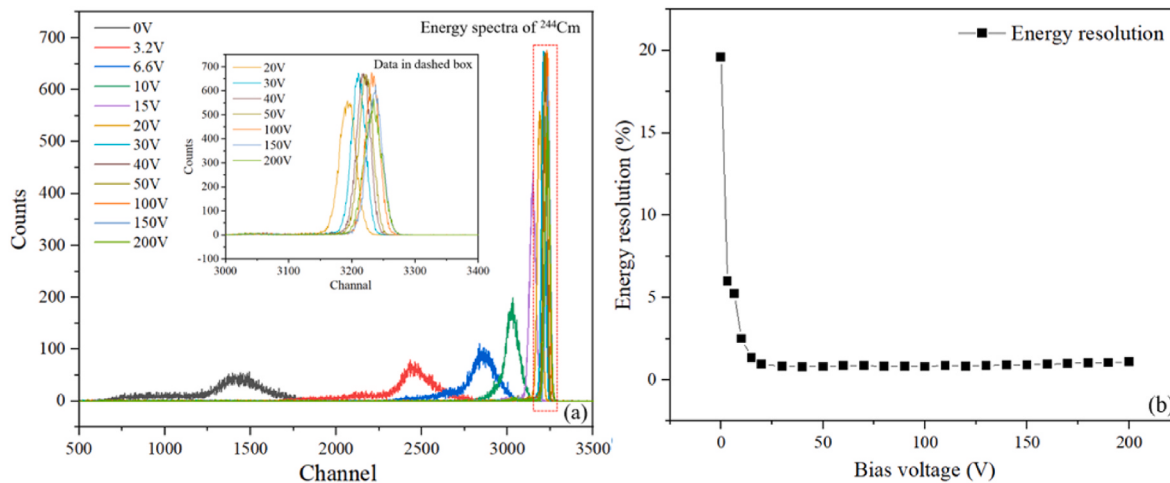


**Fig. 6.** (a)  $\alpha$ -Particle energy spectrum of the detector before irradiation at voltages ranging from 0 V to  $-200$  V. (b) Relationship between energy resolution and bias voltage.

before and after neutron irradiation. The forward and reverse J-V curves are presented in Fig. 4(a) and (b) respectively. Prior to neutron irradiation, the detector exhibited excellent electrical performance. Analysis of the forward J-V curve using the thermionic emission model yielded a turn-on voltage of 0.8 V, an ideality factor of 1.04, and a Schottky barrier height of 1.24 eV for the detector. The leakage current of the detector remained low, measuring below  $-30$  pA/cm<sup>2</sup> within the voltage range of 0 V to  $-60$  V. However, significant changes were observed in the electrical characteristics of the detector after neutron irradiation, particularly in the forward J-V characteristics. The conduction of the detector became problematic, with a turn-on voltage exceeding 15 V. Multiple measurements of the forward J-V characteristics were conducted, and it was observed that the conduction was unstable, yielding inconsistent data in repeated measurements. This is related to the damage of the metal semiconductor contact interface caused by neutron irradiation [8,37]. On the other hand, no significant changes were observed in the reverse leakage current of the detector.

The C-V curves is shown in Fig. 5. The testing frequency is 1 MHz. The detector capacitance is large due to its large sensitivity area. It can be regarded as a junction capacitance formed by the depletion region. The detector capacitance  $C_D$  can be expressed as (1):

$$C_D = \frac{SE_s}{W_D} = S\sqrt{\frac{q\epsilon_s N_D}{2}} \left( \varphi_{bi} - V - \frac{kT}{q} \right)^{-\frac{1}{2}} \quad (1)$$

where,  $S$  is detector sensitivity area,  $W_D$  is depletion region width,  $\epsilon_s$  is the permittivity of 4H-SiC,  $N_D$  is electron concentration, and  $\varphi_{bi}$  is the built-in potential of 4H-SiC. Equation (1) can be expressed as:

$$\frac{1}{C_D^2} = \frac{2\left(\varphi_{bi} - V - \frac{kT}{q}\right)}{S^2 q \epsilon_s N_D} \quad (2)$$

Prior to neutron irradiation, the  $\varphi_{bi}$  of the detector, as determined from the  $1/C^2$ -V curve, was found to be 1.76 V. The average carrier concentration in the epitaxial layer was measured to be  $1.29 \times 10^{14}$  cm<sup>-3</sup>. The discrepancy between the calculated barrier height from the J-V curve and the measured value is attributed to the non-uniformity of the Schottky barrier. Following irradiation, the capacitance of the detector remained unchanged with varying bias voltage, this phenomenon is consistent with the observation in Ref. [8]. Within the bias voltage range of 0 V to  $-25$  V, the capacitance of the detector was approximately 0.52 nF/cm<sup>2</sup>, corresponding to a depletion width of 16.7  $\mu$ m. This observation is attributed to the carrier removal effect induced by neutron irradiation [38].

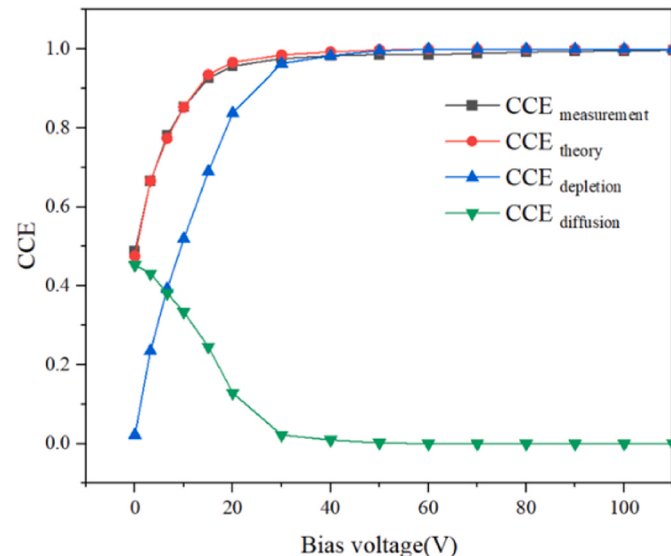


**Fig. 7.** The CCE of the 4H-SiC detector and the fitting results of the carrier drift-diffusion model.

### 3.2. Pulse height spectroscopy and CCE

To measure the energy spectrum of the 4H-SiC detector, we employed a  $^{244}\text{Cm}$   $\alpha$  source. The pulse-height spectra obtained at various bias voltages ranging from 0 V to  $-200$  V are displayed in Fig. 6(a). According to SRIM calculations, the penetration depth of 5805 keV  $\alpha$  particles in the 4H-SiC detector is determined to be 19.8  $\mu$ m. The fully depleted voltage, as derived from (1), is approximately  $-60$  V. Remarkably, the detector exhibited a response to  $\alpha$  particles even at 0 V bias voltage, indicating the ability to operate without bias. The signal amplitude saturated when the bias voltage reached  $-50$  V, and further increasing the bias voltage did not result in a higher signal amplitude. The full width at half maximum (FWHM) was extracted by fitting a Gaussian function to the pulse-height spectra. The energy spectra have been calibrated by Si detector and function generator. The energy resolution, expressed as the ratio of FWHM to the peak position, is illustrated in Fig. 6(b).

The energy resolution gradually improved with increasing bias voltage and tended to stabilize after becoming below  $-30$  V. At  $-40$  V, the optimal energy resolution reached 0.79% (45.63 keV). Moreover,

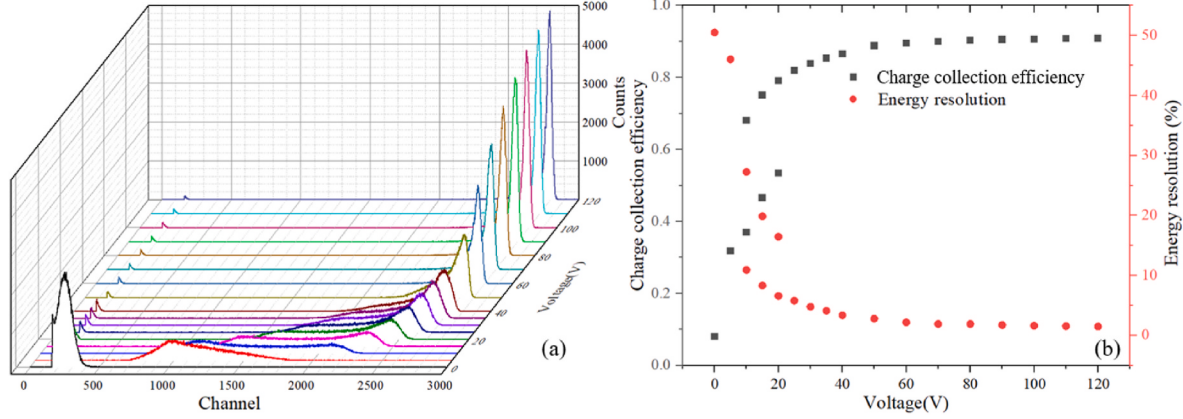


**Fig. 8.** (a)  $\alpha$ -Particle energy spectrum of the 4H-SiC detector after irradiation. (b) Relationship between CCE and energy resolution with bias voltages.

the energy resolution of the detector remained within 1% when the bias voltage was set between  $-20\text{ V}$  and  $-200\text{ V}$ .

The correlation between CCE and bias voltages is depicted in Fig. 7. To determine the individual contributions of drift ( $\text{CCE}_{\text{depletion}}$ ) and diffusion ( $\text{CCE}_{\text{diffusion}}$ ) to the CCE, we employed the drift-diffusion model described by (3) [6,39]:

$$\text{CCE}_{\text{theory}} = \frac{1}{E_{\text{ion}}} \int_0^{W_D} \left( -\frac{dE}{dx} \right) \xi(x) dx + \frac{1}{E_{\text{ion}}} \int_{W_D}^R \left( -\frac{dE}{dx} \right) \exp \left( -\frac{x - W_D}{L_p} \right) dx \quad (3)$$

where,  $E_{\text{ion}}$  is the ion energy,  $dE/dx$  is the electronic stopping power,  $\xi(x)$  is the probability of the charge generated at a distance  $x$  from the front of Schottky diode being collected by the detector,  $R$  is the incident particle range in 4H-SiC, and  $L_p$  is the minority carrier diffusion length. The first term of the (3) is the CCE in the depletion region, called  $\text{CCE}_{\text{depletion}}$ , and the second term is the charge collection due to the carrier diffusion, called  $\text{CCE}_{\text{diffusion}}$ . We used (3) to fit the CCE measurement curve, where  $L_p$  is a free parameter. The fitting outcome is presented in Fig. 7, demonstrating that the drift-diffusion calculation accurately reproduces the measured CCE. The calculated  $L_p$  is determined to be  $12.71\text{ }\mu\text{m}$ . It is slightly higher than the results obtained in other literature [6, 39,40]. This indicates that the 4H-SiC epitaxial material has extremely high crystal quality. When the bias voltage applied to the detector is low, the incident particle range significantly exceeds the width of the depletion region, causing most of the charges to be generated in the neutral region. In this case, charge collection primarily occurs through the diffusion of these charges. As the bias voltage becomes more negative than  $-6.5\text{ V}$ ,  $\text{CCE}_{\text{depletion}}$  surpasses  $\text{CCE}_{\text{diffusion}}$ , indicating that charge collection within the depletion region becomes the primary component of CCE. With increasingly negative bias voltages, the width

of the depletion region surpasses the incident particle range, resulting in CCE being predominantly governed by the charges drifting within the depletion region.

We performed spectroscopic testing on the neutron-irradiated detectors under identical conditions, and the results are illustrated in Fig. 8. Notably, a splitting of the energy spectrum was observed at bias voltages less negative than  $-25\text{ V}$ . Within the range of  $-10\text{ V}$  to  $-20\text{ V}$ , two distinct peaks were observed in the energy spectra. This splitting is attributed to the multiple capture and release of ionization-generated electron-hole pairs by defects induced through irradiation. The CCE of the detector exhibited a significant decrease without bias voltage, dropping from 47.5% to 8%. Simultaneously, the saturated CCE also experienced a slight decrease, declining from 100% to 90.8%. The energy resolution of the detector increased from 0.79% at  $-40\text{ V}$  to 1.49% at  $-120\text{ V}$  after irradiation. This observation indicates that the detector, following neutron irradiation, requires a higher bias voltage to enhance its detection efficiency, which is linked to the impact of defects. Despite the occurrence of radiation damage, the detector irradiated with a fluence of  $1.24 \times 10^{14}\text{ n/cm}^2$  still maintains low leakage current and exhibits good energy resolution capability. This demonstrates the strong radiation resistance of the 4H-SiC detector.

### 3.3. DLTS measurements

We conducted DLTS testing on the detector before and after irradiation to determine the energy levels, concentrations, and capture cross-sections of crystal defects. The DLTS results obtained before irradiation are presented in Fig. 9. The bias voltage applied to the detector was  $U_r = -10\text{ V}$ , the pulse voltage was  $U_p = -0.5\text{ V}$ , and the pulse duration was  $t_p = 100\text{ ms}$ . Initially, the rate window  $t_w$  was fixed for temperature scanning, and after neutron irradiation,  $t_w$  was modified to obtain the peak temperature corresponding to different rate windows. Fig. 9(a)

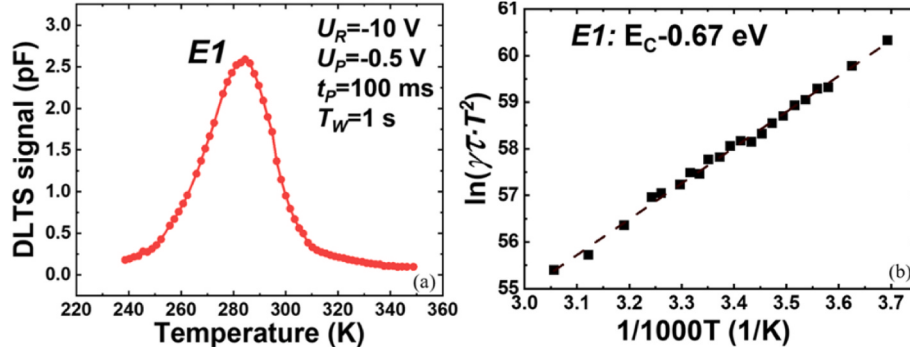


**Fig. 9.** DLTS results of the detector before irradiation. (a) Temperature scan with a fixed rate window of 1 s. (b) Data extraction at different temperature peaks.

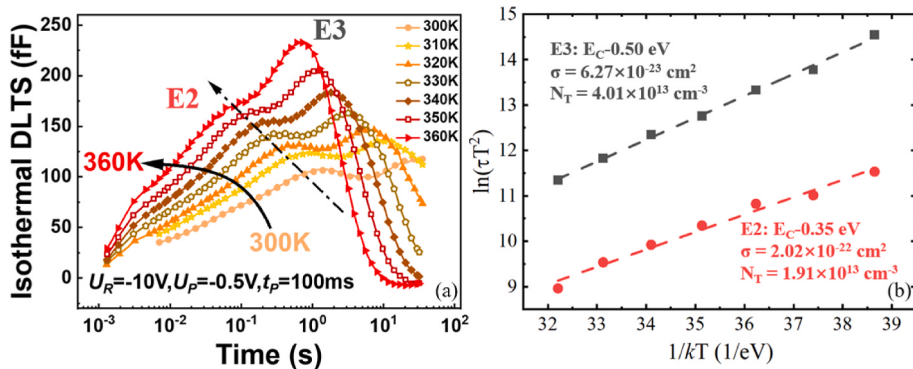


**Fig. 10.** DLTS results of the detector after irradiation. (a) Rate window scan with temperatures ranging from 300 K to 360 K. (b) Data extraction at different rate window peaks.

**Table 2**  
DLTS results of the detector before and after irradiation.

	Energy level (eV)	Capture cross-section (cm²)	Trap concentration (cm⁻³)	Condition
E1	$E_c - 0.67 \pm 0.01$	$2.07 \times 10^{-14}$	$3.31 \times 10^{14}$	Pristine
E2	$E_c - 0.35 \pm 0.03$	$6.27 \times 10^{-23}$	$1.91 \times 10^{13}$	Irradiated
E3	$E_c - 0.50 \pm 0.03$	$2.02 \times 10^{-22}$	$4.01 \times 10^{13}$	Irradiated

displays the DLTS signal spectrum with a rate window of 1 s. Based on the dynamic equilibrium process of carrier capture and emission by crystal defects, Equation (4) can be derived [41].

$$\ln(\gamma\tau T^2) = \frac{E}{kT} + \ln(-\sigma_n) \quad (4)$$

In the equation,  $\tau$  represents the rate window ( $t_w$ ),  $\sigma_n$  is the capture cross-section,  $E$  is the activation energy, and  $\gamma = \frac{4\sqrt{6}k^2\pi^{3/2}m_n^*}{h^3}$  is a constant related to the material properties. By varying the rate window, the curve shown in Fig. 9(b) can be obtained. Performing a linear fit on  $\ln(\gamma\tau T^2) - \frac{1}{1000T}$  curve, the slope and intercept can be extracted, yielding a defect energy level of  $E_c - 0.67$  eV in the pre-irradiated material, corresponding to a capture cross-section of  $2.07 \times 10^{-14}$  cm<sup>2</sup>. This is a common defect level found in 4H-SiC epitaxial materials. It has been explained in various ways in previous reports, including silicon vacancies, carbon vacancies, divacancy complexes, and di-interstitial complexes. Among these explanations, the carbon vacancy theory is predominant, and the influence of this defect can be reduced by providing a carbon-rich environment. This defect exhibits thermal stability above 1700 °C and is positively correlated with the net doping concentration in the epitaxial layer. Due to the carrier removal effect caused by neutron irradiation, this defect cannot be measured in materials after neutron irradiation [27,28,42–45]. The DLTS results after neutron irradiation are shown in Fig. 10.

After irradiation, the DLTS spectrum reveals two new defect energy levels:  $E_c - 0.35$  eV and  $E_c - 0.50$  eV. Their concentration is lower than the concentration of the E1 level. The results are summarized in Table 2. According to previous reports, these two defect levels may correspond to  $Z_2^{0/+}$  and  $Z_1^{0/+}$  structures [27,29,46]. They are the defect structures after the  $Z_{1/2}$  defect loses its charges. These defects can be generated by irradiation with 470 nm light [29]. In the irradiation experiment of this paper, the white neutron source is from the scattering reaction of high-energy protons with a tungsten target. Therefore, the neutron beam is accompanied by a large amount of gamma radiation. In this paper, the 4H-SiC detector received a gamma radiation fluence of  $3.31 \times 10^{13}$   $\gamma/cm^2$ . It is possible that the irradiation of gamma rays changed the

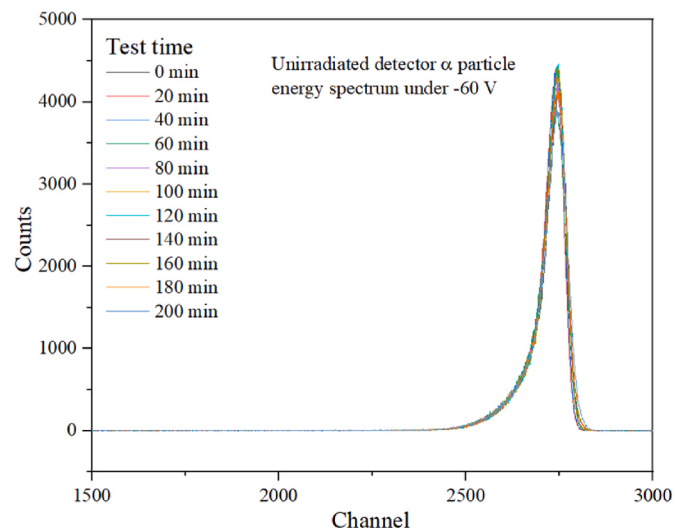


**Fig. 11.** Long-term alpha particle energy spectrum of the detector before irradiation.

charge state of the carbon vacancy defect, thus forming the E2 and E3 levels. Therefore, the performance changes of the detector after irradiation are the result of the combined effects of neutron irradiation and gamma ray irradiation. These defects have the ability to capture free electrons, resulting in a reduction of the net doping concentration in the epitaxial layer and causing the detector to exhibit a high-resistive state in its electrical characteristics. Furthermore, in other reports, there are more speculations about the origin and defect structure of the E2 and E3 levels. These include vacancy defects [19,47], impurity atom interstitials [26] (such as the injection of surface electrode Ti atoms), and vacancy-interstitial complex defects [28]. Currently, there are no fully reliable results in the reports, and more in-depth research is needed to confirm the detailed information.

### 3.4. Polarization effect

The polarization effect in semiconductor detectors refers to the phenomenon where the energy spectrum of the detector drifts and the counting rate decreases during long-term charged particle measurements. This is caused by the change in the electric field distribution of the depletion region due to the trapping of charge carriers by defects. Neutron irradiation can create crystal defects in semiconductor materials, which may act as trap centers to capture and release charge carriers, or as recombination centers to recombine electron-hole pairs. When the defects capture the charge carriers, the charge becomes fixed

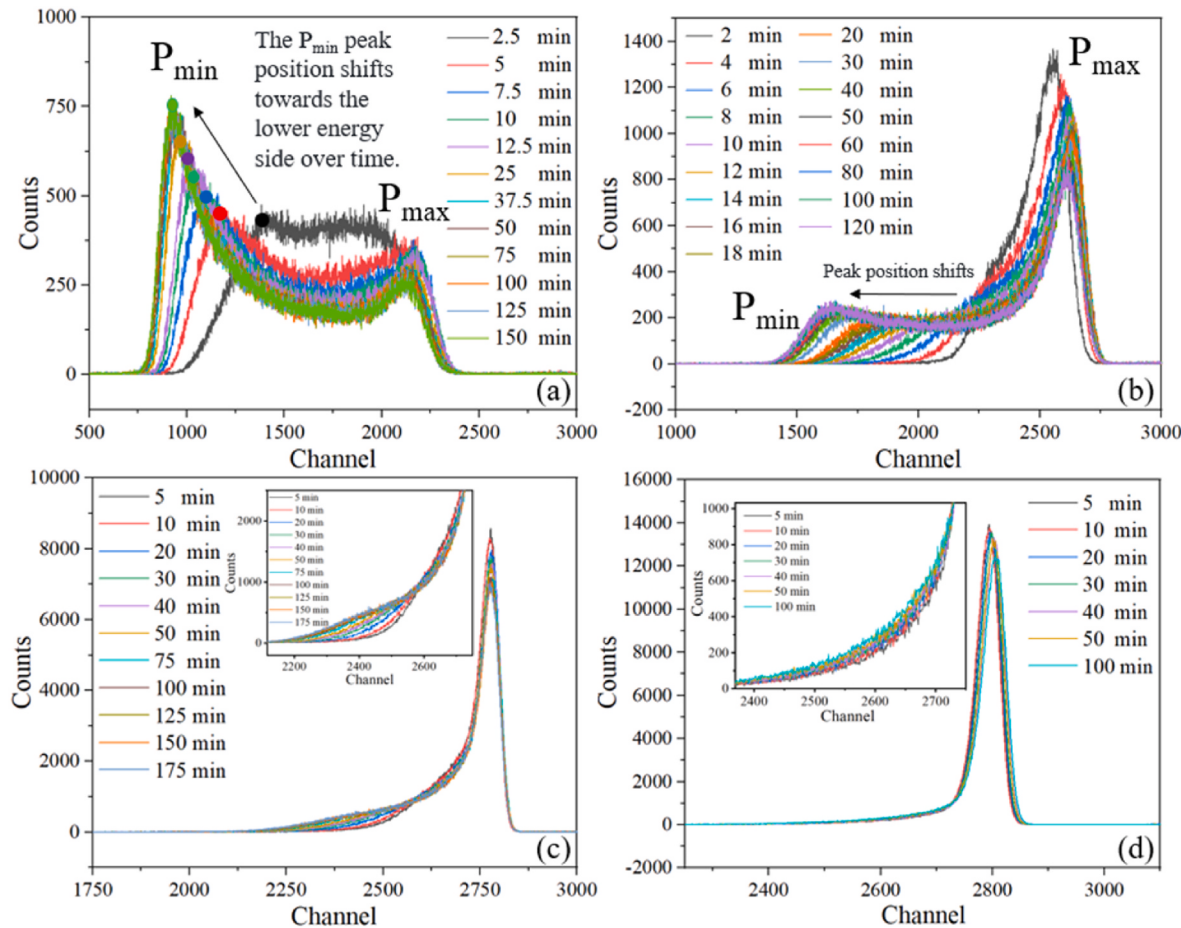


**Fig. 12.** The neutron-irradiated detector was used to measure the alpha particle energy spectrum of the  $^{241}\text{Am}$  source. The detector performed cyclic and continuous energy spectrum measurements at different bias voltages. The measurement time for a single energy spectrum was 2 min. The bias voltages of the detector were (a)  $-10$  V, (b)  $-30$  V, (c)  $-60$  V, and (d)  $-100$  V. The inset is a magnified view of the energy spectrum variation.

as the defect cannot move. This causes a decrease in the output signal amplitude of the detector, leading to spectrum drift. Additionally, after capturing charge carriers for a period of time, trap centers will release the charge carriers again. When the trapping rate is greater than the release rate, the detector accumulates fixed charges, and the polarization effect gradually strengthens. When the trapping rate is equal to the release rate, the fixed charge density reaches a dynamic equilibrium, and the detector reaches a state of polarization saturation. After removing the radiation source, the release rate becomes greater than the trapping rate, causing the fixed charge density to decrease, and the detector enters a process of polarization recovery [32].

Firstly, a prolonged energy spectrum analysis was conducted on a non-irradiated detector using a  $^{244}\text{Cm}$  alpha source. The test was conducted at a temperature of 300 K. The detector was biased at  $-60$  V, and the energy spectra were collected cyclically, with each testing cycle lasting 2 min. A total of 100 cycles were performed, and the outcomes are illustrated in Fig. 11. Throughout the entire measurement, the detector exhibited stability, with no discernible alterations observed in the shape, position, full width at half maximum (FWHM), or any other energy spectrum characteristics.

Following irradiation, we proceeded with a subsequent long-term energy spectrum analysis to monitor the temporal changes. The experiment was carried out under vacuum and light-avoidance conditions, with an incident rate of 6700  $\alpha/\text{s}$ . The bias voltage was adjusted within the range of  $-10$  V to  $-100$  V. Fig. 12 illustrates the evolution of the energy spectra over time at various bias voltages.

It is evident that the irradiated detector exhibits an inability to maintain stable operation over an extended duration. The distortion of

the energy spectrum and the decline in peak position during the initial testing period are indicative of typical polarization effects. The electric field intensity within the space charge region diminishes, resulting in a significant reduction in CCE. Additionally, we observed the occurrence of energy spectrum splitting. Following the incidence of a monoenergetic  $\alpha$  particle, the energy spectrum splits into two peaks: one with higher energy ( $P_{\max}$ ) and the other with lower energy ( $P_{\min}$ ). This phenomenon is particularly prominent at lower bias voltages. In the early phases of irradiation, the majority of counts are concentrated in  $P_{\max}$ . As the irradiation progresses, counts appear to shift from  $P_{\max}$  to  $P_{\min}$ , until  $P_{\min}$  becomes the dominant spectrum and stabilizes. During the polarization process, the peak intensity of  $P_{\max}$  decreases, the count of  $P_{\min}$  gradually increases, and at the same time, the peak position of  $P_{\min}$  shifts towards the lower energy side. This indicates that as the polarizing electric field is generated, fewer charge carriers are able to pass through the polarized region and be fully collected. This behavior, previously observed by M. Hodgson and Souw in diamond detectors, indicates a gradual filling of traps within the material with the generated charge carriers, reaching a saturation point [32,33]. Once saturation is achieved, a stable electric field and corresponding energy spectrum are maintained.

At higher bias voltages (more negative than  $-60$  V), the electric field intensity within the space charge region can be maintained at a high level. This reduces the likelihood and duration of charge carrier capture by defects, thereby minimizing its impact on CCE. As shown in Fig. 12 (d), the energy spectrum's shape and position remain largely unchanged over time. This observation suggests that the neutron-irradiated 4H-SiC detector can still be effectively utilized in experiments. However, it is

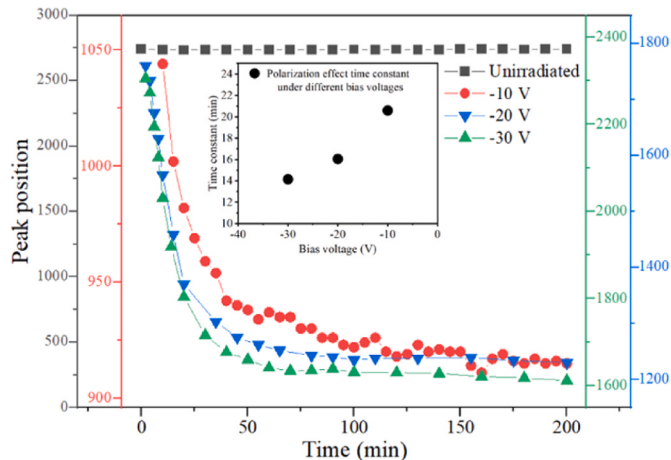


**Fig. 13.** The variation of energy spectra peak position with test time for the detector before and after irradiation at different bias voltages.

**Table 3**  
Polarization effect results of the detector before and after irradiation.

	Initial amplitude (channel)	Time constant (min)	Descend ratio
Unirradiated	2740	—	—
-10V	1044	20.59	12.36%
-20V	1760	16.05	28.83%
-30V	2305	14.15	29.93%

necessary to appropriately increase the bias voltage to ensure stable detector operation.

We have analyzed the relationship between the  $P_{\min}$  peak position of the energy spectrum test and time for the detector biased at  $-10$  V to  $-30$  V, and the results are summarized in Fig. 13. At different voltages, the peak position of the energy spectrum exhibits an exponential decay trend over time. By fitting the curves, we can obtain the decay time constant, which represents the rate at which the detector achieves stable operation and reflects the influence of bias voltage on the polarization effect. The experimental results are summarized in Table 3. It is observed that higher bias voltages allow the detector to reach a stable operating state more quickly. However, simultaneously, it also leads to a more significant decrease in the peak position of the energy spectrum. A possible reason could be that higher bias voltage reduces the

concentration of defects occupied by the charge carriers under the dynamic balance between capture and emission, thereby reducing the time constant. Within the range of  $-10$  V to  $-30$  V, the detector is in a partially depleted state. Increasing the bias voltage enhances the detector's CCE, but it also amplifies the impact of the polarization effect on CCE, resulting in a greater decrease in the peak position.

In addition, we conducted measurements on the recovery process of polarization effects. Once the detector reached a stable state after complete polarization, we removed the bias voltage and continued monitoring the time-dependent energy spectrum of the detector at 0 V. The variation of the energy spectrum is presented in Fig. 14. At this stage, the emission rate of carriers from defects exceeds the capture rate, leading to the depolarization process of the detector. After approximately 15 min, the energy spectrum of the detector returned to an unpolarized state. It is evident that the influence of alpha particle irradiation on the polarization recovery process of the detector cannot be avoided. Although there is no drift electric field within the space charge region, carriers can still diffuse and be captured and emitted by defects. Hence, these tests may not accurately reflect the emission rate of defects, but they do provide insights into the recovery of the detector and offer some guidance for its usage.

#### 4. Conclusion

The impact of neutron irradiation on semiconductor detectors is multifaceted, as it induces internal crystal defects that can significantly affect the electrical characteristics and charge collection capabilities of the detector. However, as a wide bandgap semiconductor, 4H-SiC exhibits remarkable radiation resistance. Even after neutron irradiation at a fluence of  $1.24 \times 10^{14}$  n/cm<sup>2</sup>, the detector's charge collection capability experiences minimal degradation, with the energy resolution still maintained at 1.49%. These findings indicate that the 4H-SiC detector can reliably operate in high-dose irradiation environments. This radiation resistance enables 4H-SiC detectors to perform tasks that are challenging for Si detectors, such as measuring zero-degree differential cross-sections of nuclear reactions [14], particle identification in high-fluence composite radiation fields as a dE-E detector [48] and other high flux environments detection [15].

Furthermore, we have observed the presence of polarization effects in neutron-irradiated epitaxial 4H-SiC Schottky detectors. Previous reports [34,35,49] have mainly focused on thicker detectors based on single-crystal materials, where polarization effects were commonly observed. However, the underlying cause of polarization effects remains the same, which is the long-term trapping of charge carriers by crystal defects. Therefore, neutron irradiation damage to 4H-SiC detectors not

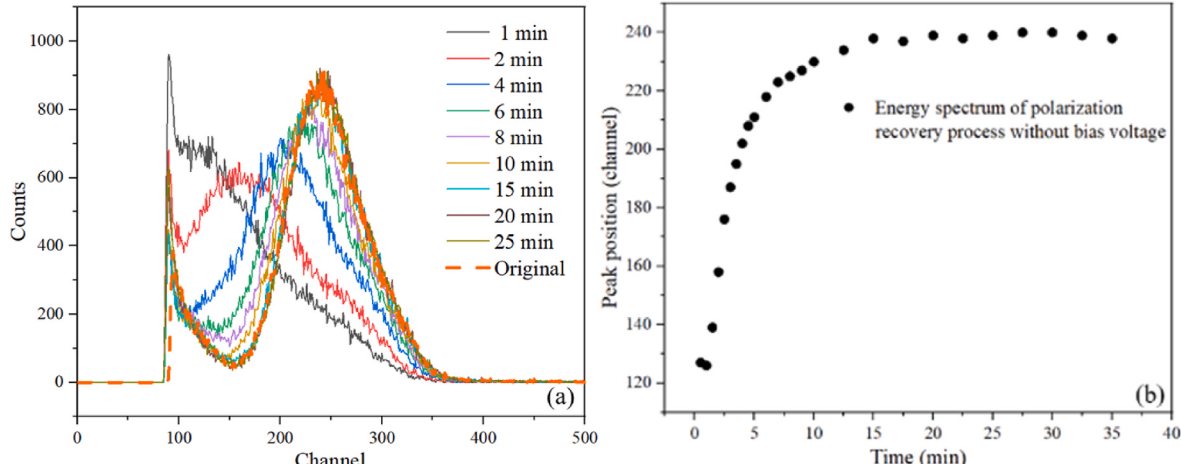


**Fig. 14.** After the 4H-SiC detector reaches a stable polarized state, the bias voltage is removed to measure the recovery process of the detector's polarization. (a) Variation of energy spectrum recovery with time at zero bias voltage. (b) Relationship between energy spectrum peak position and recovery time.

only results in degradation of energy collection and resolution but also leads to a deterioration in detector stability. In this study, we experimentally demonstrated that increasing the bias voltage of the detector effectively mitigates the impact of polarization effects. Neutron-irradiated detectors operated at  $-120$  V exhibit minimal degradation in detection performance, and no energy spectrum shift caused by polarization effects was observed.

## CRediT authorship contribution statement

**Ze Long:** Writing – original draft, Software, Methodology, Investigation, Formal analysis, Data curation, Conceptualization. **Xiaochuan Xia:** Writing – review & editing, Investigation. **Wei Jiang:** Writing – review & editing, Investigation. **Hantao Jing:** Investigation, Writing – review & editing. **Xinbo Zou:** Writing – review & editing, Data curation. **Xin Shi:** Writing – review & editing, Data curation, Conceptualization. **Mengchen Niu:** Writing – review & editing, Investigation, Data curation. **Hongwei Liang:** Writing – review & editing, Supervision, Funding acquisition, Conceptualization. **Ruirui Fan:** Supervision, Methodology, Funding acquisition, Data curation, Conceptualization, Writing – review & editing.

## Declaration of competing interest

The authors declare that they have no known competing financial interests or personal relationships that could have appeared to influence the work reported in this paper.

## Data availability

Data will be made available on request.

## Acknowledgment

This work was supported by the National Natural Science Foundation of China under Grant 12075045, Grant 1875097, Grant 11975257, Grant 62074146, the Strategic Priority Research Program of the Chinese Academy of Sciences, Grant No. XPB2302, the Fundamental Research Funds for the Central Universities under Grant DUT22LK23, Grant DUT21RC(3)014, the Natural Science Foundation of Liaoning Province under Grant 2020MS243 and the Ministry of Industry and Information Technology of the People's Republic of China.

## References

- [1] I. Capan, 4H-SiC Schottky barrier diodes as radiation detectors: a review, *Electronics* 11 (4) (2022) 1–12.
- [2] L.Y. Liu, L. Wang, P. Jin, et al., The fabrication and characterization of Ni/4H-SiC Schottky diode radiation detectors with a sensitive area of up to  $4\text{ cm}^2$ , *Sensors* 17 (10) (2017) 1–9.
- [3] K.C. Mandal, J.W. Kleppinger, S.K. Chaudhuri, Advances in high-resolution radiation detection using 4H-SiC epitaxial layer devices, *Micromachines* 11 (3) (2020) 1–27.
- [4] L. Zhang, Y.H. Meng, J.T. Li, et al., Fabrication of a 4H-SiC p-i-n diode Array for high energy particle detection, *IEEE Trans. Electron. Dev.* 69 (9) (2022) 2103–2107.
- [5] K.C. Mandal, S.K. Chaudhuri, K. Nguyen, An overview of application of 4H-SiC n-type epitaxial Schottky barrier detector for high resolution nuclear detection, *NSS/MIC*, Seoul, Korea (2013) 1–6.
- [6] J. Wu, Y. Jiang, J.R. Lei, et al., Effect of neutron irradiation on charge collection efficiency in 4H-SiC Schottky diode, *Nucl. Instrum. Methods Phys. Res. Sect. A Accel. Spectrom. Detect. Assoc. Equip.* 735 (2014) 218–222.
- [7] B. Zat'ko, et al., Particle detectors based on 4H-SiC epitaxial layer and their properties, *ASDAM*, Smolenice, Slovakia (2016) 141–144.
- [8] L.Y. Liu, T.L. Shen, A. Liu, et al., Performance degradation and defect characterization of Ni/4H-SiC Schottky diode neutron detector in high fluence rate neutron irradiation, *Diam. Relat. Mater.* 88 (2018) 256–261.
- [9] J. Wu, M. Li, Y. Jiang, et al., Performance of a 4H-SiC Schottky diode as a compact sized detector for neutron pulse form measurements, *Nucl. Instrum. Methods Phys. Res. Sect. A Accel. Spectrom. Detect. Assoc. Equip.* 771 (2015) 17–20.
- [10] F.H. Ruddy, L. Ottaviani, A. Lyoussi, et al., Silicon carbide neutron detectors for harsh nuclear environments: a review of the state of the art, *IEEE Trans. Nucl. Sci.* 69 (4) (2022) 792–803.
- [11] F.H. Ruddy, J.G. Seidel, The effects of intense gamma-irradiation on the alpha-particle response of silicon carbide semiconductor radiation detectors, *Nucl. Instrum. Methods Phys. Res. Sect. B Beam Interact. Mater. Atoms* 263 (2007) 163–168.
- [12] F.H. Ruddy, J.G. Seidel, Effects of gamma irradiation on silicon carbide semiconductor radiation detectors, in: 2006 IEEE Nuclear Science Symposium Conference Record, 2006, pp. 583–587. San Diego, CA, USA.
- [13] A.R. Dulloo, F.H. Ruddy, J.G. Seidel, et al., The thermal neutron response of miniature silicon carbide semiconductor detectors, *Nucl. Instrum. Methods Phys. Res. Sect. A Accel. Spectrom. Detect. Assoc. Equip.* 498 (2003) 415–423.
- [14] Z. Long, M.C. Niu, X.C. Xia, et al., Development of the large sensitive area 4H-SiC Schottky detectors at the Back-n, *Nucl. Instrum. Methods Phys. Res. Sect. A Accel. Spectrom. Detect. Assoc. Equip.* 1056 (2023) 1–5.
- [15] J.M. Raft, et al., Electron, neutron, and proton irradiation effects on SiC radiation detectors, *IEEE Trans. Nucl. Sci.* 67 (12) (2020) 2481–2489.
- [16] E.V. Kalinina, A.A. Lebedev, E. Bogdanova, et al., Irradiation of 4H-SiC UV detectors with heavy ions, *Semiconductors* 49 (2015) 540–546.
- [17] H. Li, C. Liu, Zhang, et al., Irradiation effect of primary knock-on atoms on conductivity compensation in N-type 4H-SiC Schottky diode under various irradiations, *Semicond. Sci. Technol.* 34 (9) (2019).
- [18] L.Y. Liu, A. Liu, S. Bai, et al., Radiation resistance of silicon carbide Schottky diode detectors in D-T fusion neutron detection, *Sci. Rep.* 7 (2017) 1–8.
- [19] L.Y. Liu, F.P. Li, S. Bai, et al., Silicon carbide PIN diode detectors used in harsh neutron irradiation, *Sens. Actuators, A* 280 (2018) 245–251.
- [20] P. Hazdra, S. Popelka, V. Zahlava, et al., Radiation damage in 4H-SiC and its effect on power device characteristics, *Solid State Phenom.* 242 (2015) 421–426.
- [21] P. Kandlakunta, C. Tan, N. Smith, et al., Silicon carbide detectors for high flux neutron monitoring at near-core locations, *Nucl. Instrum. Methods Phys. Res. Sect. A Accel. Spectrom. Detect. Assoc. Equip.* 953 (2020) 1–8.
- [22] D.S. Chao, H.Y. Shih, J.Y. Jiang, et al., Influence of displacement damage induced by neutron irradiation on effective carrier density in 4H-SiC SBDs and MOSFETs, *Jpn. J. Appl. Phys.* 58 (2019) 1–8.
- [23] E. Kalinina, G. Kholyanov, A. Strel'chuk, et al., Electrical study of fast neutron irradiated devices based on 4H-SiC CVD epitaxial layers, *Mater. Sci. Forum* 457–460 (2004) 705–708.
- [24] R.L. Gao, X. Du, W.Y. Mac, et al., Radiation tolerance analysis of 4H-SiC PIN diode detectors for neutron irradiation, *Sensor Actuator A-Phys* 333 (2021) 1–7.
- [25] B. Zat'ko, et al., Spectrometric performance of 4H-SiC detectors after neutron irradiation, *APCOM*, Smolenice, Slovakia 2778 (2023).
- [26] J.P. Doyle, M.O. Abelfotoh, M.K. Linnarsson, et al., Characterization of deep level defects in 4H and 6H SiC via DLTS, SIMS and MeV E-beam irradiation, in: *Symposium on III-Nitride, SiC and Diamond Materials for Electronic Devices*, San Francisco, USA, vol. 423, 1996, pp. 519–524.
- [27] N.T. Son, X.T. Trinh, L.S. Løvlie, et al., Negative-U system of carbon vacancy in 4H-SiC, *Phys. Rev. Lett.* 109 (18) (2012) 1–5.
- [28] T.A.G. Eberlein, R. Jones, P.R. Briddon,  $Z_1/Z_2$  defects in 4H-SiC, *Phys. Rev. Lett.* 90 (22) (2003) 1–4.
- [29] C.G. Hemmingsson, N.T. Son, A. Ellison, et al., Negative-U centers in 4H silicon carbide, *Phys. Rev. B* 58 (16) (1998) 10119–10122.
- [30] P. Hazdra, J. Vobecky, Radiation defects created in n-type 4H-SiC by electron irradiation in the energy range of 1–10 MeV, *Phys. Status Solidi A* 216 (17) (2019) 1–7.
- [31] A. Castaldini, A. Cavallini, L. Rigutti, et al., Low temperature annealing of electron irradiation induced defects in 4H-SiC, *Appl. Phys. Lett.* 85 (2004) 3780–3782.
- [32] M. Hodgson, A. Lohstroh, P. Sellin, Alpha radiation induced space charge stability effects in semi-insulating silicon carbide semiconductors compared to diamond, *Diam. Relat. Mater.* 78 (2017) 49–57.
- [33] E.K. Souw, R.J. Meilunas, Response of CVD diamond detectors to alpha radiation, *Nucl. Instrum. Methods Phys. Res. Sect. A Accel. Spectrom. Detect. Assoc. Equip.* 400 (1) (1997) 69–86.
- [34] S. Mohapatra, M. Abhangi, S. Vala, et al., Comparative study of Single Crystal (SC)-Diamond and 4H-SiC bulk radiation detectors for room temperature alpha spectroscopy, *J. Instrum.* 16 (2021) p06020.
- [35] G. Bertuccio, D. Puglisi, A. Pullia, et al., X- $\Gamma$  ray spectroscopy with semi-insulating 4H-silicon carbide, *IEEE Trans. Nucl. Sci.* 60 (2) (2013) 1436–1441.
- [36] R.R. Fan, et al., Detection of low-energy charged-particle using the  $\Delta E$ - $E$  telescope at the Back-n white neutron source, *Nucl. Instrum. Methods Phys. Res. Sect. A Accel. Spectrom. Detect. Assoc. Equip.* 981 (2020) 1–7.
- [37] A. Castaldini, A. Cavallini, F. Nava, et al., Electron induced damage effects in 4H-SiC Schottky diodes, *Mater. Sci. Forum* 433–436 (2003) 439–442.
- [38] A.A. Lebedev, A.M. Ivanov, N.B. Strokan, Radiation resistance of SiC and nuclear-radiation detectors based on SiC films, *Semiconductors* 38 (2) (2003) 129–150.
- [39] J.W. Kleppinger, S.K. Chaudhuri, O. Karadavut, et al., Defect characterization and charge transport measurements in high-resolution Ni/n-4H-SiC Schottky barrier radiation detectors fabricated on  $250\text{ }\mu\text{m}$  epitaxial layers, *J. Appl. Phys.* 129 (24) (2021) 1–10.
- [40] F. Nava, E. Vittonne, P. Vanni, et al., Radiation tolerance of epitaxial silicon carbide detectors for electrons, protons and gamma-rays, *Nucl. Instrum. Methods Phys. Res. Sect. A Accel. Spectrom. Detect. Assoc. Equip.* 505 (2003) 645–655.
- [41] D.R. Yang, *DLTS Measurement. Semiconductor Material Testing And Analysis*, Beijing, PR China, first ed., 2010, pp. 182–194. ch. 7, sec. 2.

- [42] T. Dalibor, G. Pensl, H. Matsunami, et al., Deep defect centers in silicon carbide monitored with deep level transient spectroscopy, *Phys. Status Solidi A* 162 (1) (1997) 119–225.
- [43] A. Kawasuso, et al., Annealing behavior of vacancies and Z<sub>1/2</sub> levels in electron-irradiated 4H-SiC studied by positron annihilation and deep-level transient spectroscopy, *Appl. Phys. Lett.* 79 (24) (2001) 3950–3952.
- [44] A.A. Lebedev, D.V. Davydov, N.S. Savkina, et al., Structural defects and deep-level centers in 4H-SiC epilayers grown by sublimational epitaxy in vacuum, *Semiconductors* 34 (10) (2000) 1183–1186.
- [45] M. Kato, Yoshihara Ki, M. Ichimura, et al., Observation of deep levels and their hole capture behavior in p-type 4H-SiC epilayers with and without electron irradiation, *Jpn. J. Appl. Phys.* 53 (4) (2014) 1–5.
- [46] A. Cavallini, A. Castaldini, F. Nava, Deep levels in 4H silicon carbide epilayers induced by neutron-irradiation up to 10<sup>16</sup> n/cm<sup>2</sup>, *Mater. Res. Soc. Symp. Proc.* (2006) 237. USA.
- [47] T. Dalibor, C. Peppermuller, G. Pensl, et al., Defect centers in ion-implanted 4H silicon carbide, *Silicon Carbide And Relat Mater* 142 (1995) 517–520.
- [48] C. Ciampi, G. Pasquali, C. Altana, et al., Nuclear fragment identification with ΔE-E telescopes exploiting silicon carbide detectors, *Nucl. Instrum. Methods Phys. Res. Sect. A Accel. Spectrom. Detect. Assoc. Equip.* 925 (2019) 60–69.
- [49] P. Vigneshwara Raja, J. Akhtar, C.V.S. Rao, et al., Spectroscopic performance studies of 4H-SiC detectors for fusion alpha-particle diagnostics, *Nucl. Instrum. Methods Phys. Res. Sect. A Accel. Spectrom. Detect. Assoc. Equip.* 869 (2017) 118–127.